Electronic Supplementary Material (ESI) for ChemComm.

Supporting Information

Unveiling the active sites of Ni-Fe phosphide/metaphosphate for efficient oxygen evolution under alkaline condition

Can Huang,[a] Ying Zou,[a] Ya-Qian Ye, [a] Ting Ouyang,[a] Kang Xiao[a] and Zhao-Qing Liu*[a]

[a]*School of Chemistry and Chemical Engineering/Institute of Clean Energy and Materials, Guangzhou University, Guangzhou Higher Education Mega Center, No. 230 Wai Huan Xi Road, 510006, P. R. China. E-mail: lzqgzu@gzhu.edu.cn*

Contents

1. Experimental Section

2. Supplementary Figures and Table

1. Experimental Section

1.1 Chemicals

All reagents used in the experiment are of analytical grade and used without further purification. $Ni(NO_3)_2 \cdot 6H_2O$ (99% AR), $Fe(NO_3)_3 \cdot 9H_2O$ (98.5% AR), Na_2CO_3 (99.8% AR) are obtained from Guangzhou Chemical Reagent Factory. RuO_2 (75% wt.) is obtained from Shanghai Hansi Chemical Industry Co., Ltd.. Polyvinylpyrrolidone (PVP, 99% AR) are obtained from Shanghai Tianlian Fine Chemical Co. Ltd.. The multi-walled carbon nanotubes (CNT, 99% AR) are purchased from Shenzhen Nanotech Port Co. Ltd..

1.2 Synthesis of Materials

1.21 Synthesis of functionalization of carbon nanotubes (fCNTs): fCNTs was prepared by a modified Hummers method.[1] Briefly, 23 mL concentrated sulfuric acid was added to CNTs and stirred for overnight. Then, 416 mg of KNO_3 was added, followed by the slow addition of 1 g of $KMnO_4$ in ice-bath. The mixture was kept stirring at 40 ℃ for 30 min. Subsequently, 3 mL of de-ionized (DI) water was added to the flask, followed by another 3 mL of DI water after 3 minutes. After another 3 minutes, 40 mL of DI water was added. After continuously stirring for 30 minutes, 140 mL of DI water and 10 mL of H_2O_2 (30 %) were added to terminate the oxidization reaction. The oxidized CNTs were collected, repetitively washed with 5 % HCl solution and DI water, and finally lyophilized. Additional solvothermal step for 2g oxidized CNTs added in 50 mL concentrated sulfuric acid was applied to remove metal ions and surface fragment carbon. Then, functionalized CNTs were washed by DI water for several times until pH approach to neutral. Lastly, the sample was collected after lyophilization.

1.22 Synthesis of $Ni_{1-x}Fe_x$-O_x@fCNTs: Generally, 70 mg fCNTs were dispersed in 195 mL ethanol by ultrasonic for 30 min. Next $Ni(NO_3)_2 \cdot 6H_2O$ and $Fe(NO_3)_3 \cdot 9H_2O$ in total 1 mmol with various ratio were added to the suspension, followed by addition of 5 mL of 1 M Na_2CO_3 at room temperature. The reaction is kept at 80 °C with stirring for 20 h. After that, the mixture was transferred to 100 mL autoclave for solvothermal reaction at 150 °C for 1 h. The resulting product is collected by centrifugation and washed with ethanol and water, and dried by lyophilization.

1.23 Synthesis of $Ni_{1-x}Fe_x$-P/PO_3@fCNTs: To prepare $Ni_{1-x}Fe_x$-P/PO_3@fCNTs, corresponding $Ni_{1-x}Fe_x$-O_x@fCNTs and NaH_2PO_2 were put at two separate positions in alundum boat. The mass ratio for $Ni_{1-x}Fe_x$-O_x@fCNTs and NaH_2PO_2 was 1:10. After flushed with Ar for several times, the center of the furnace was elevated to 650 °C at a ramping rate of 1 °C min^{-1} and held this temperature for 2 h. The as-prepared $Ni_{1-x}Fe_x$-P/PO_3@fCNTs was collected after naturally cool down to room temperature under Ar.

1.24 Synthesis of $Ni_{1-x}Fe_x$-P/PO_3: $Ni_{1-x}Fe_x$-P/PO_3 without fCNTs was synthesized in same approach with $Ni_{1-x}Fe_x$-P/PO_3@fCNTs except adding fCNTs.

***1.3 Characterizations*:** The morphology of materials were analyzed by field emission scanning electron microscopy (FE-SEM, JEOL JSM-7001F) and transmission electron microscopy (TEM, JEOL JEM-2100F). The crystal structure of the as-prepared samples was analyzed by X-ray diffraction (XRD, PANalytical, PW3040/60) with Cu Kα radiation (λ = 0.15418 nm). Detailed chemical composition of samples was analyzed by X-ray photoelectron spectroscopy (XPS, ESCALab250), and the binding energies were normalized by C 1s peak at 284.6 eV from adventitious carbon. For the post-CV and chronopotentiometry XPS mesurement, catalysts

were deposit on the carbon cloth, and the integrate carbon cloth after CV and chronopotentiometry was directly used for XPS measurement.

1.4 Electrochemical Measurements

1.41 Electrode preparation: Electrochemical analysis was performed under identical conditions with the same catalyst mass loading in a standard operation as reported by T.F. Jaramillo et al.[2] Briefly, 5 mg of the as-synthesized catalyst was first ultrasonically dispersed in a mixture of 0.38 mL DI water and 0.1 mL 2-propanol followed by the addition of 4 µL of Nafion® solution (5.0 wt%). Then, 6.1 µL of the catalyst dispersion (10.33 mg mL^{-1}) was transferred onto the mirror-polished glassy carbon rotating disk electrode (RDE, 0.126 cm^2) with a loading of 0.5 mg cm^{-2}, following by solvent evaporation in 60 °C for 10 min. The resulting electrode was served as the working electrode.

1.42 Electrochemical testing: The electrochemical properties of the as-prepared samples were investigated using an AMETEK Princeton Applied Research ParSTAT MC 1000 equipped with a rotation disk electrode (PINE, glassy carbon, 0.126 cm^{-2}). Typical three-electrode system was employed in 1 M KOH (pH = 14). A graphite rod serves as a counter electrode, Hg/HgO electrode as the reference electrode and the RDE as working electrodes operating at 1600 rpm. All potentials were converted to reversible hydrogen electrode (RHE) following the equation:

$$E_{RHE}\,(V) = E_{Hg/HgO} + 0.924\,V$$

The overpotential (η) for OER was calculated as:

$$\eta\,(V) = E(Hg/HgO) - 0.306\,V$$

Polarization and CV curves were recorded at the scan rate of 5 mV s^{-1}. All sulution resistance (R_s) were compensated by the *IR* compensation which measured by Electrochemical

impedance spectroscopy (EIS). The measured R_s were all in the small region from 2.5 to 3.7 Ω, and all test procedure were in accordance under same test system. Therefore, we chose the average value of 3.0 Ω as the compensating resistance, and the compensation ratio was 80%. EIS was performed at working potential in the frequency range of 1 Hz to 100000 Hz.

1.43 Chronopotentiometry measurements: Chronopotentiometry test was performed with the same three-electrode setup as mentioned before. In order to reduce the liquid pressure on the surface of electrode, rotate speed was adjusted to 1000 rpm under current density of 10 mA cm^{-2}.

1.44 Parallel electrochemical experiment used for XPS measurement: It should be noted that one of Auger peak for fluoride is located at 859.0 eV which is included in Ni 2p spectrum (~852–870 eV) and the polymer covering could reduce the signal of interior catalyst. Therefore, parallel experiment was simultaneously applied on carbon cloth under megnetic stirring with catalyst loading of 1 mg cm^{-2} and Nafion-free. $Ni_{1-x}Fe_x$-P/PO_3@fCNTs on carbon cloth was washed and lyophilized after CV and chronopotentiometry measurement to do next XPS test.

1.45 Electrochemical active surface area (ECSA): Electrochemical capacitance was measured through a series of CV measurements with different scan rate. The scaning region was chose within a narrow potential window which no faradaic current was observed. CV curves were collected at different scan rates: 5, 10, 20, 30, 40, and 50 mV s^{-1}. The different current at center point was mostly contributed by the charging of the double-layer which was proportion to the electrochemical active surface areas. By plotting the capacitive currents ($\Delta j = j_a - j_c$) against the scan rate and following with a linear fit, the double layer capacitance C_{dl} is around half of the slope. The ECSA can be further estimated from C_{dl} normalized by a specific capacitance for a flat surface, which is normally between 20-60 μF cm^{-2}. Here we used

40 μF cm^{-2} as the standard for the ECSA estimation and the turnover frequency calculation in section 1.4.6.

1.46 Turnover frequency (TOF) calculations: TOF was calculated by a previous method, [3] according to the following formula:

$$\mathrm{TOF} = \frac{\text{Number of total hydrogen (or oxygen) turn overs / geometric area (cm2)}}{\text{Number of active sites / geometric area (cm2)}} \quad \textbf{(1)}$$

The number of the total oxygen turn overs can be calculated based on the current density (*j*, *IR*-corrected) according to:

$$\text{Number of O2} = j \times \frac{1C\,s^{-1}}{1000\,mA} \times \frac{1\,mol\,e}{96485.3\,C} \times \frac{1\,mol\,\mathrm{O2}}{4\,mol\,e} \times \frac{6.022 \times 1023\ \text{O2 molecules}}{1\,mol\,\mathrm{O2}}$$

$$= j \times 1.56 \times 1015\ \text{O2 molecules}\ mA^{-1}s^{-1} \quad \textbf{(2)}$$

Because the exact number of surface-active sites is ambiguous, thus, we estimated the surface metal sites as the number of surface-active sites including Ni and Fe atoms.

The active sites per real surface area is calculated from the following formula:

$$\text{Number of active sites} = \left(\frac{\text{Number of surface atoms / unit cell}}{\text{Volume / unit cell}}\right)^{\frac{2}{3}} \quad \textbf{(3)}$$

For the purpose of simplifying analysis procedure, we hypothesize the resultant after CV measurement is Ni-Fe oxyhydroxides and the in-situ generated NiOOH was stepwise transformed into FeOOH by increasing Fe content. It was approximated to the smaller Ni^{3+} in NiOOH substituted by the larger Fe^{3+} gradually. Finally, it transforms into FeOOH with the substitution ratio increased to 100%, which lead the cell enlarged but structure retained (see figures below).

Therefore, the number of active sites for $Ni_{1-x}Fe_x$-P/PO_3@fCNTs can be calculated as:

$$\text{Number of active sites (Ni1 - xFex - P/PO3@fCNTs)} = \left(\frac{2\ \text{atoms / unit cell}}{58.7 + 6.8\text{x}\ \text{Å}^3\ \text{/ unit cell}}\right)^{\frac{2}{3}} \quad \textbf{(4)}$$

Finally, substitute the current density *j* into formula above, TOF can be calculated as:

$$\text{TOF (Ni1 - xFex - P/PO3@fCNTs)} = j \times \frac{1.56 \times 10^{15}\ \text{O}_2\ \text{molecules}\ mA^{-1}\ s^{-1}}{\text{Number of active sites} \times A_{ECSA}} \quad \textbf{(5)}$$

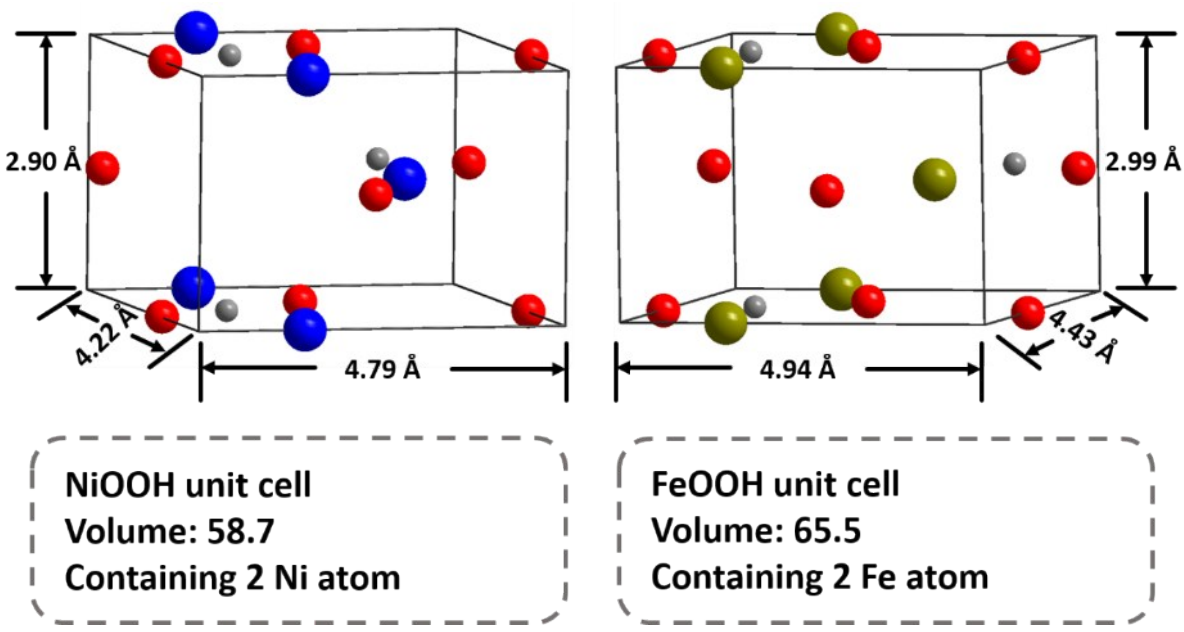

2. Supplementary Figures

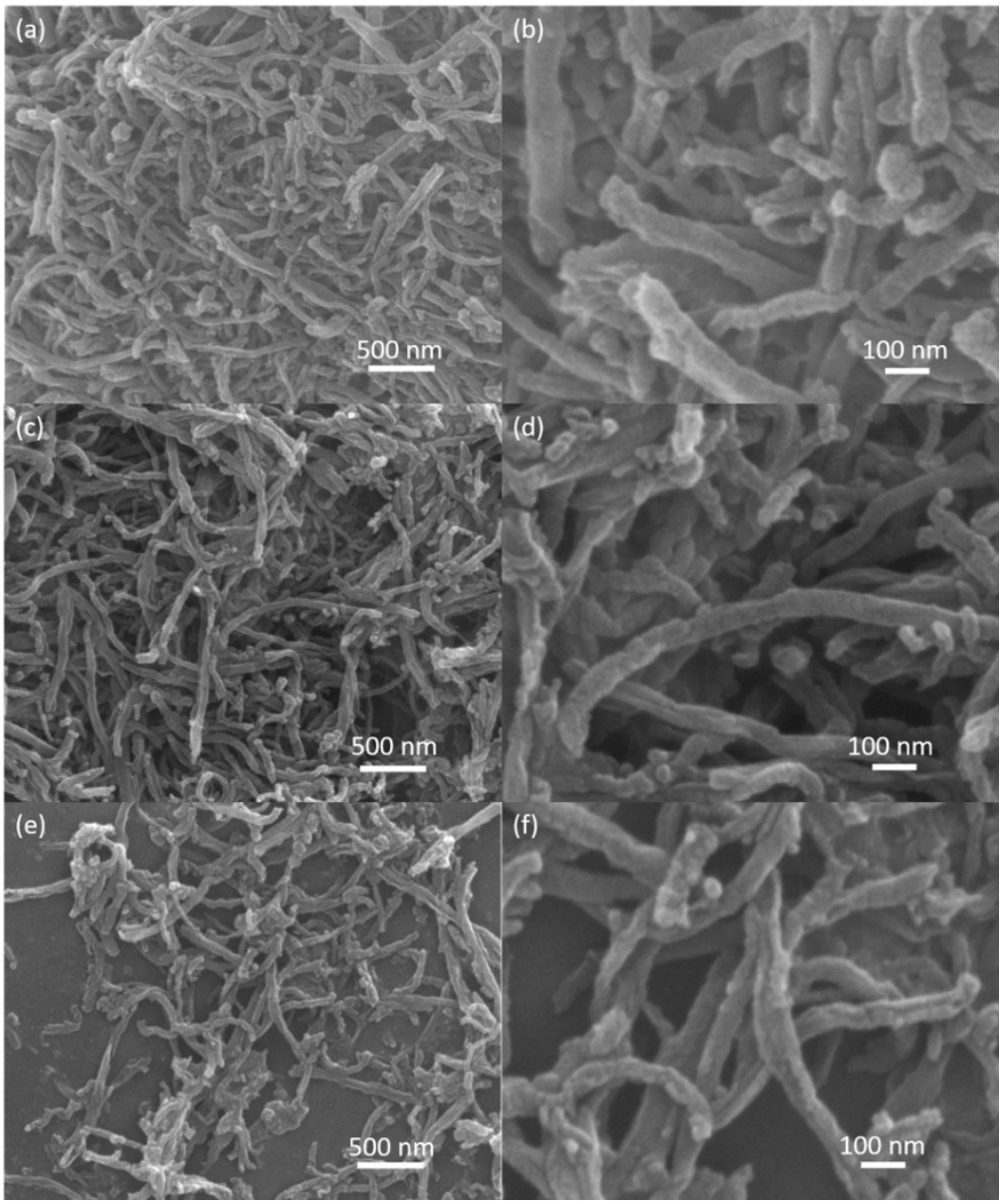

Figure S1. SEM images of (a-b) $Fe(PO_3)_2$@fCNTs, (c-d) $Ni_{0.1}Fe_{0.9}$-P/PO_3@fCNTs and (e-f) $Ni_{0.25}Fe_{0.75}$-P/PO_3@fCNTs.

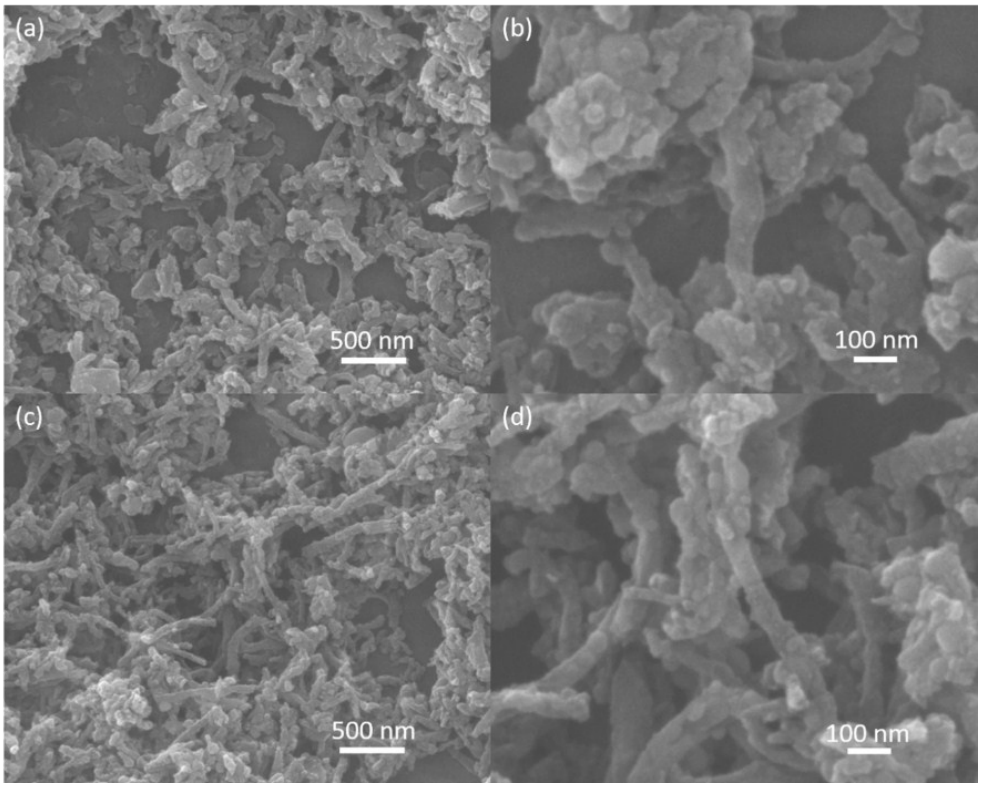

Figure S2. SEM images of (a-b) $Ni_{0.5}Fe_{0.5}$-P/PO_3@fCNTs, and (c-d) $Ni_{0.75}Fe_{0.25}$-P/PO_3@fCNTs.

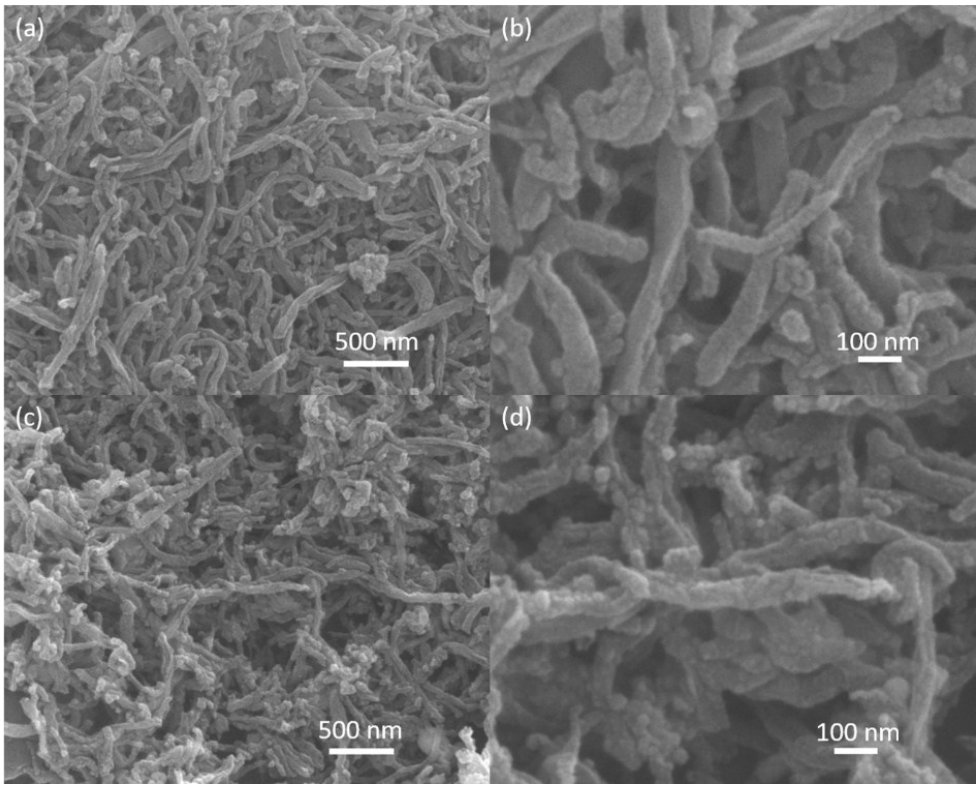

Figure S3. SEM images of (a-b) $Ni_{0.9}Fe_{0.1}$-P/PO_3@fCNTs and (c-d) Ni_2P@fCNTs.

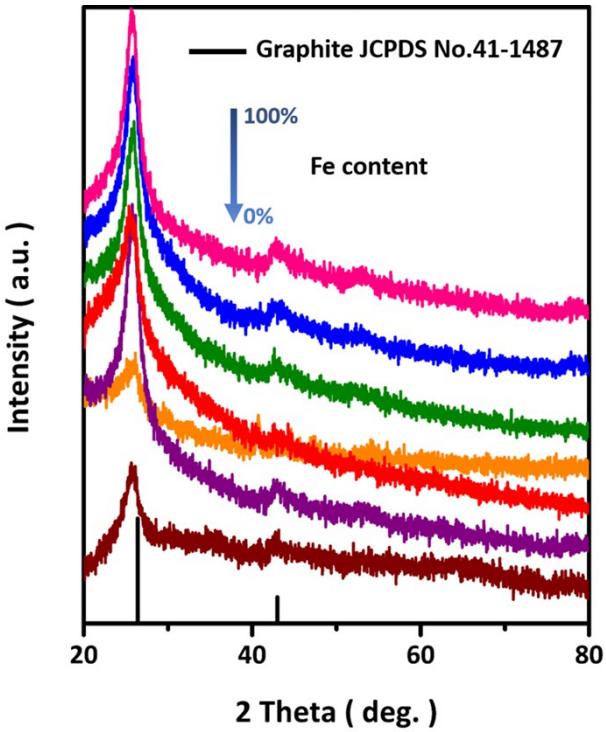

Figure S4. Powder X-ray diffraction spectra of $Ni_{1-x}Fe_x$-P/PO_3@fCNTs.

The (111) plane in Ni_2P lattice is gradually shifted to the left, when the value of Fe doping changes from 0 to 0.25, and disappears after x = 0.5. The (–113) plane in $Fe(PO_3)_2$ appears after x = 0.5, and gradually shifts to the left with x changes from 0.5 to 1. The above results demonstrate that the larger atomic sized Fe atom gradually replaced the smaller sized Ni atom.

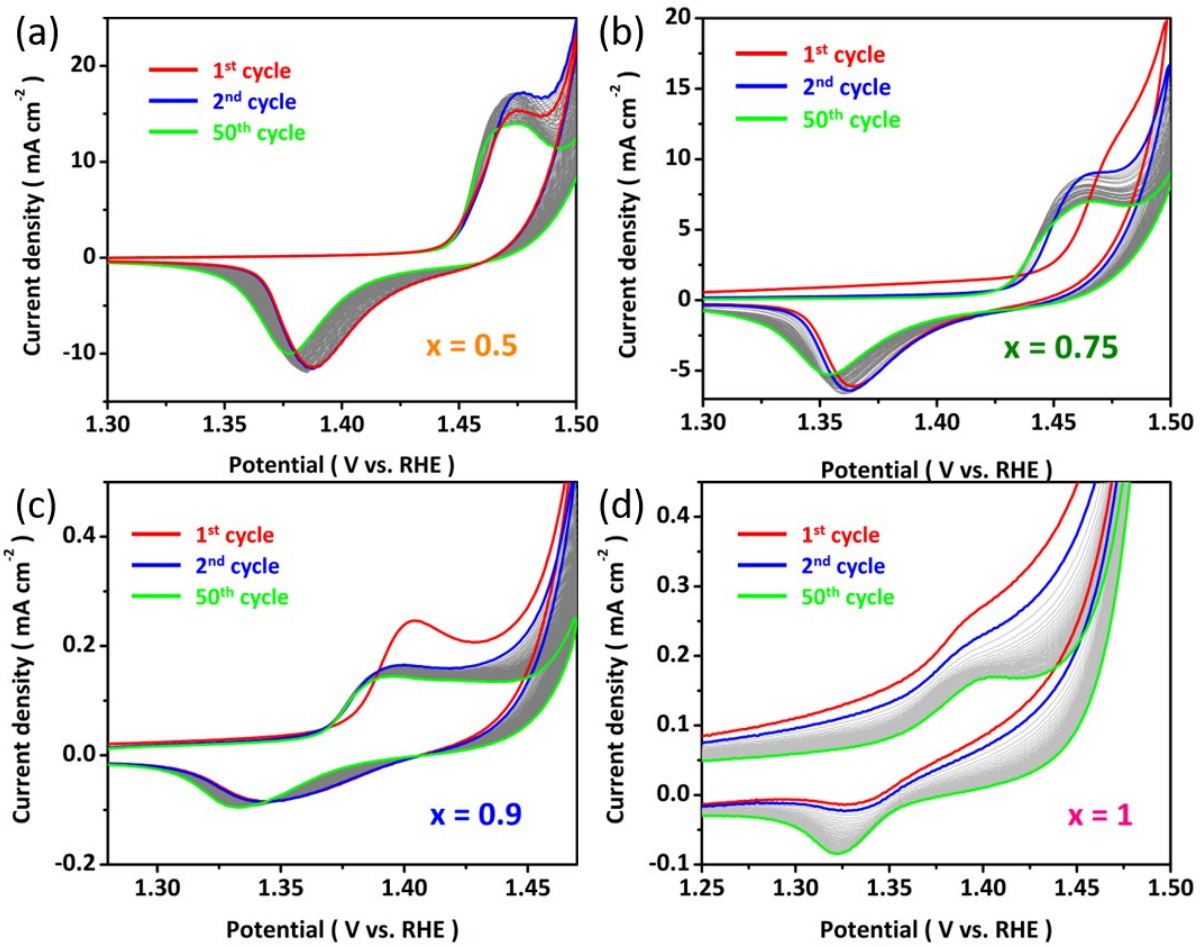

Figure S5 CV curves from 1st to 50th cycle of $Ni_{1-x}Fe_x$-P/PO_3@fCNTs catalysts with x = 0.5 – 1.

To research the interfacially chemical variation in real-time, typical CV technology can be employed to record the oxidization/reduction peak which can describe their surface variation during electrochemical process. The peak area was in proportion to the number of particular active substance, and the peak location shift could reflect the *in-situ* variation of active substance. Accordingly, CV measurement was applied to gain insight into the process of electrochemical phase transformation.

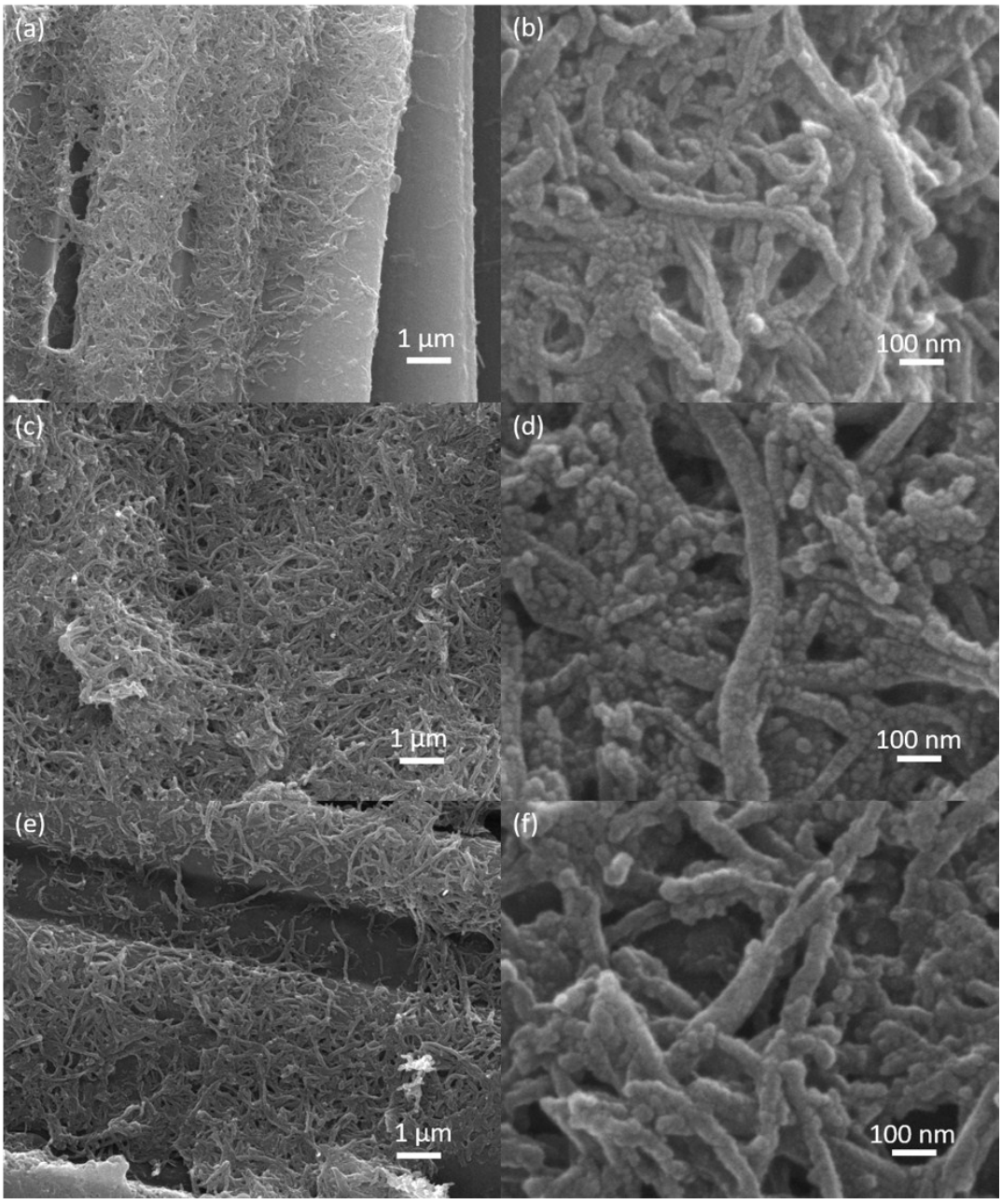

Figure S6. SEM images of (a-b) $Fe(PO_3)_2$@fCNTs, (c-d) $Ni_{0.1}Fe_{0.9}$-P/PO_3@fCNTs and (e-f) $Ni_{0.25}Fe_{0.75}$-P/PO_3@fCNTs after CV test.

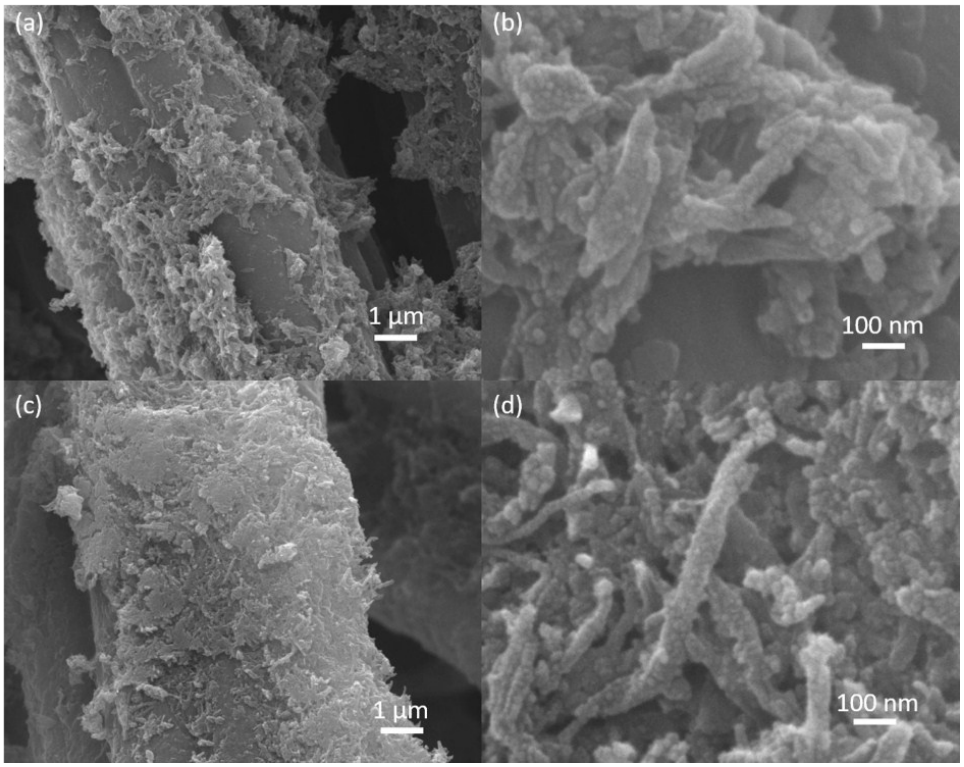

Figure S7. SEM images of (a-b) $Ni_{0.5}Fe_{0.5}$-P/PO_3@fCNTs and (c-d) $Ni_{0.75}Fe_{0.25}$-P/PO_3@fCNTs after CV test.

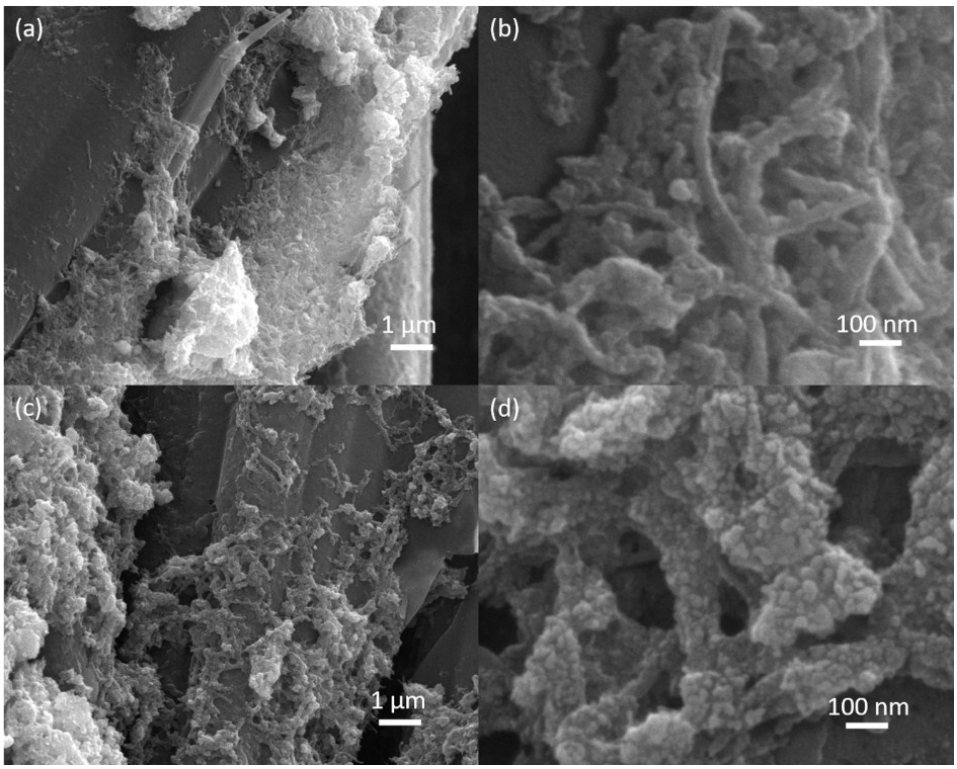

Figure S8. SEM images of (a-b) $Ni_{0.9}Fe_{0.1}$-P/PO_3@fCNTs, and (c-d) Ni_2P@fCNTs after CV test.

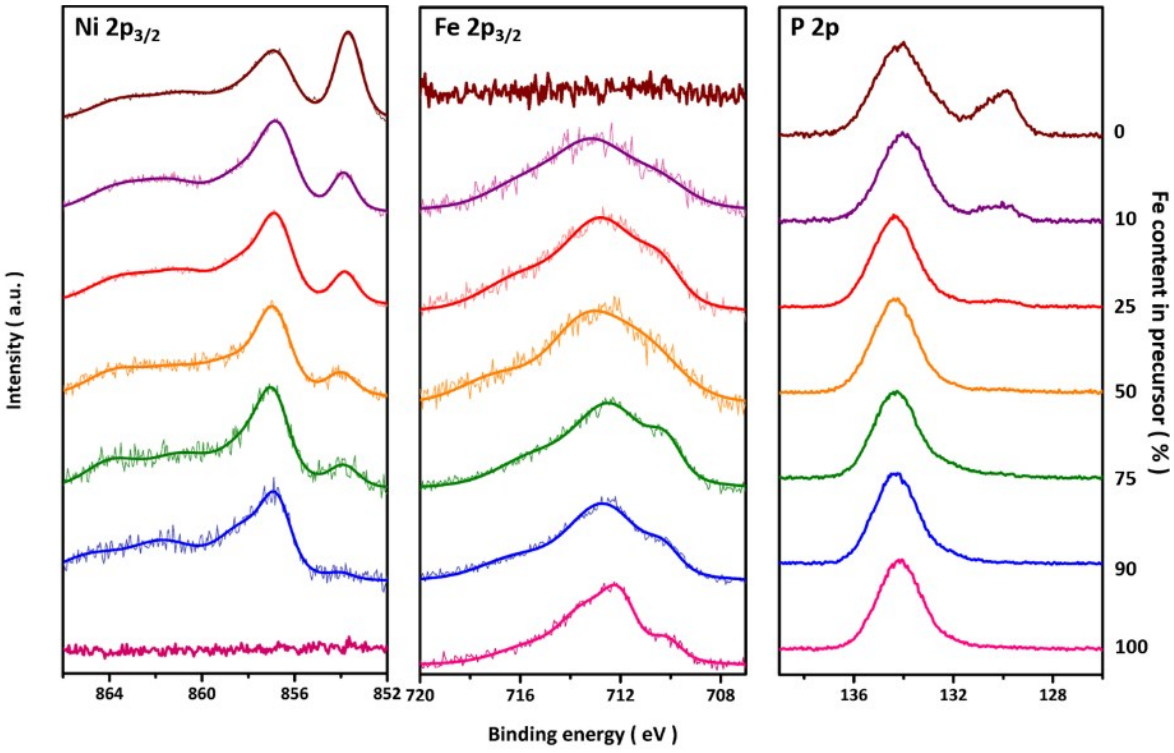

Figure S9. XPS curves of Ni $2p_{3/2}$, Fe 2p and P 2p spectra for various ratio of pristine $Ni_{1-x}Fe_x$-P/PO_3@fCNTs catalysts.

In order to prove the chemical changes after CV test, surface sensitive XPS technology was implemented to probe the chemical-state transformation of $Ni_{1-x}Fe_x$-P/PO_3@fCNTs. The testing depth of XPS is within 5–10 nm which can effectively characterize the interface and exclude the interference of body-phase.

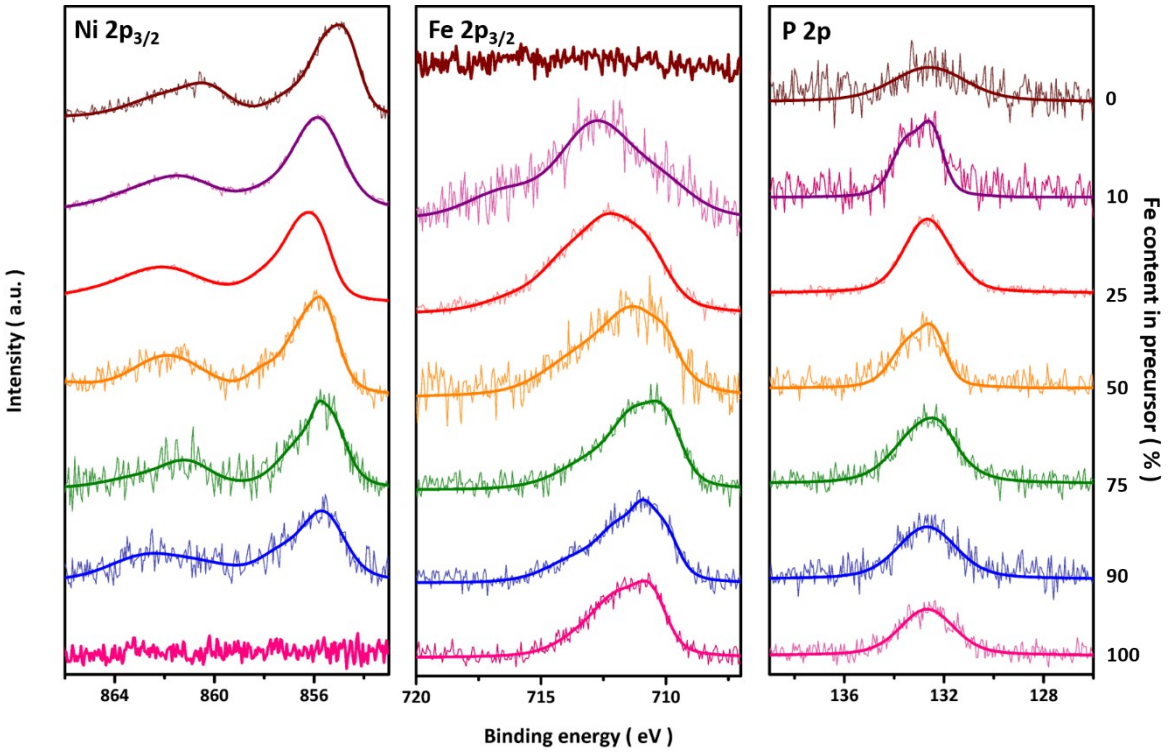

Figure S10. XPS curves of Ni $2p_{3/2}$, Fe 2p and P 2p spectra for various ratio of $Ni_{1-x}Fe_x$-P/PO_3@fCNTs catalysts after CV test.

To further explore the surface valence conversion after CV measurement, we mainly focus on the major peak to estimate the chemical valence of dominating Ni and Fe species.

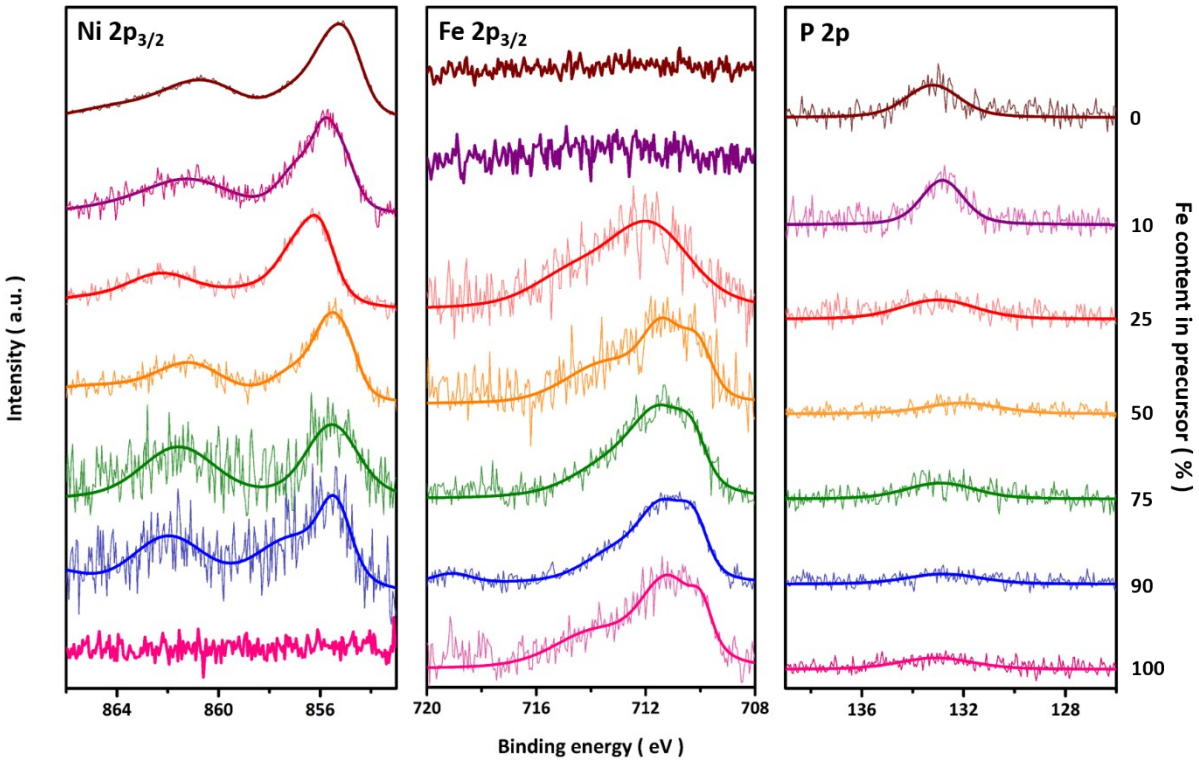

Figure S11. XPS curves of Ni $2p_{3/2}$, Fe 2p and P 2p spectra for various ratio of $Ni_{1-x}Fe_x$-P/PO_3@fCNTs catalysts after chronopotentiometry test.

The atomic interaction between Ni and Fe could only slightly affect average chemical valence in the same oxyhydroxide phase. Therefore, such highly BE shift could be attributed to their different phase after electrochemical activation.

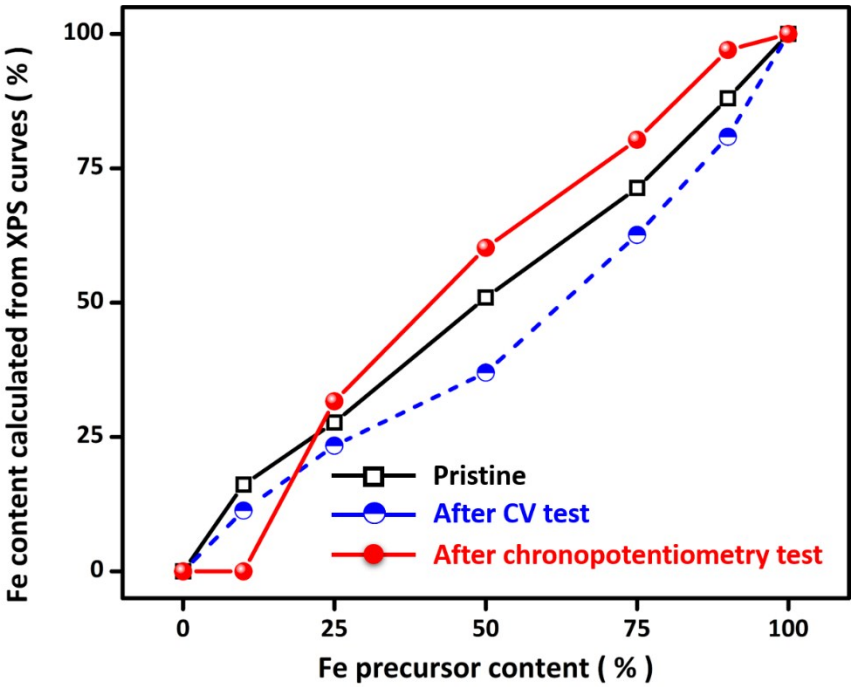

Figure S12. Exact Fe ratio of pristine, after CV test and chronoamperometry test calculated from XPS data for various ratio of $Ni_{1-x}Fe_x$-P/PO_3@fCNTs catalysts;

The overall Fe/Ni ratio can be strictly calculated by semi-quantitative analysis of XPS with background and relative sensitivity factor (RSF) calibrated. The actual surface Fe/Ni ratios of pristine $Ni_{1-x}Fe_x$-P/PO_3@fCNTs catalysts show that they were mostly identical to the precursor ratios (**Figure 3c**). The actual surface Fe/Ni ratios of $Ni_{1-x}Fe_x$-P/PO_3@fCNTs catalysts after CV measurement were lower than that of pristine catalysts, primarily because the deposited NiOOH is the dominating activated substance during the CV activation process. The actual surface Fe/Ni ratios of $Ni_{1-x}Fe_x$-P/PO_3@fCNTs catalysts test after CP test were beyond the pristine status when $x \geq 0.25$ and undetectable when $x = 0.1$. Apparently, competitive reaction for deposition of Fe and Ni ions are existed before reach their steady state. Insufficient Fe content of $Ni_{0.9}Fe_{0.1}$-P/PO_3@fCNTs would lead to slower deposition rate of Fe, then the dominating Ni element becomes the major components after CP test. On the contrary, $Ni_{0.1}Fe_{0.9}$-P/PO_3@fCNTs only maintained 3.0% Ni element after CP test.

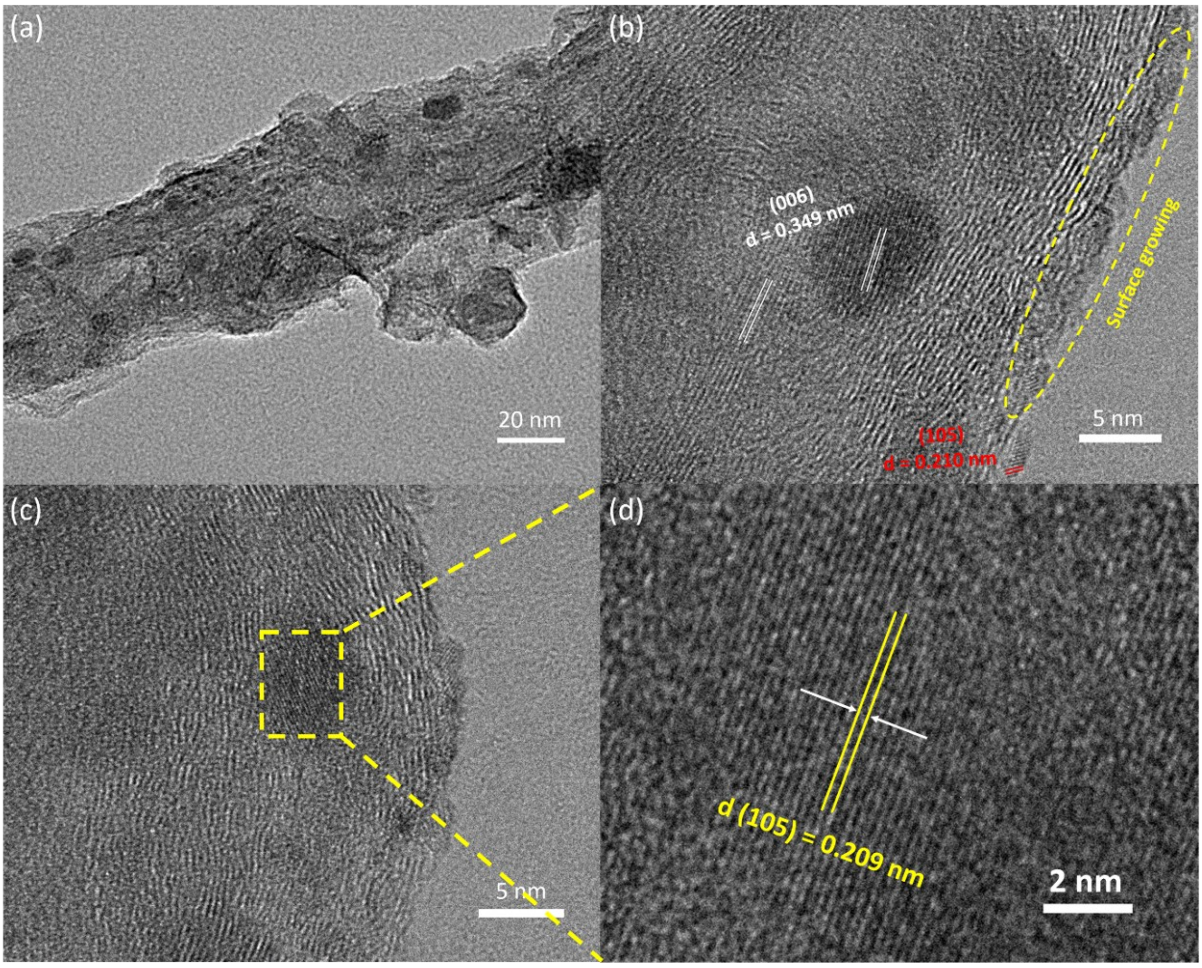

Figure S13. (a) TEM image, (b-d) HRTEM image of $Ni_{0.75}Fe_{0.25}$-P/PO_3@fCNTs after CV test.

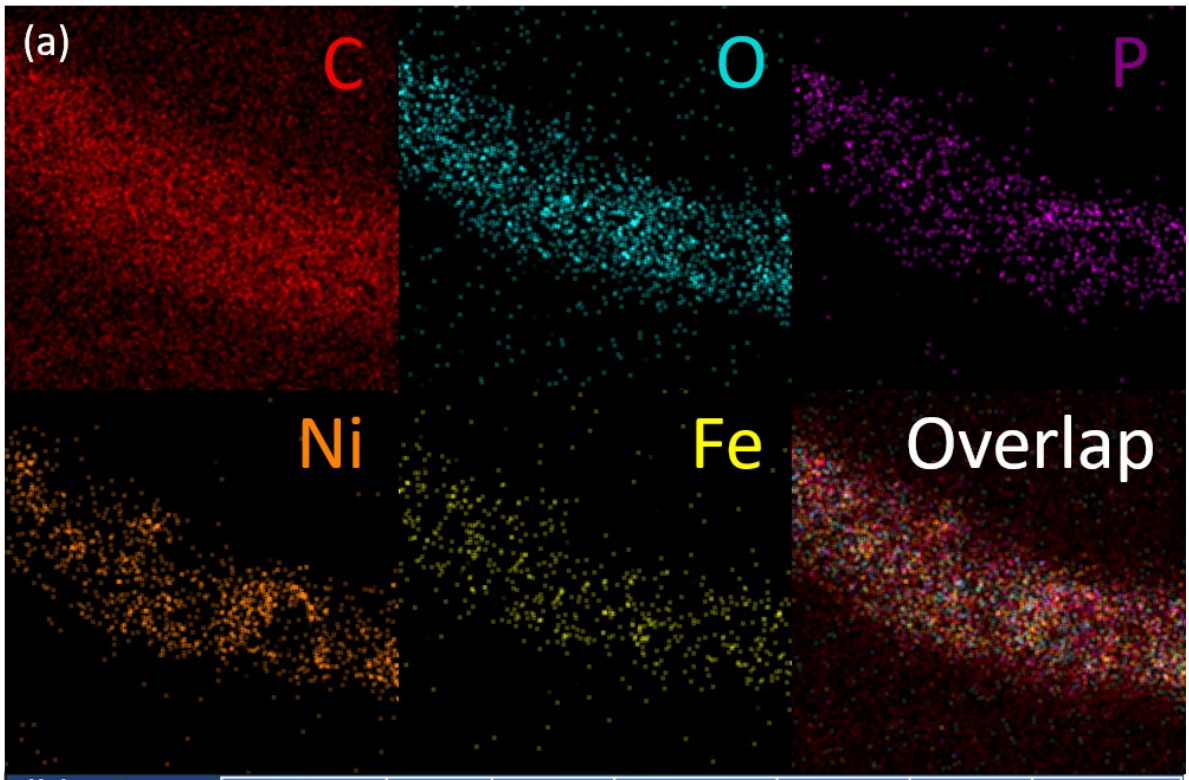

(b)

Element	Line Type	k Factor	Absorption Correction	Wt%	Wt% Sigma	Atomic %
C	K series	2.769	1.00	94.70	0.13	96.96
O	K series	2.020	1.00	3.22	0.11	2.48
P	K series	1.052	1.00	0.66	0.04	0.26
Fe	K series	1.143	1.00	0.45	0.03	0.10
Ni	K series	1.164	1.00	0.96	0.05	0.20
Total:				100.00		100.00

Figure S14. (a) EDS mapping and (b) corresponding spectrum of $Ni_{0.75}Fe_{0.25}$-P/PO_3@fCNTs after CV test.

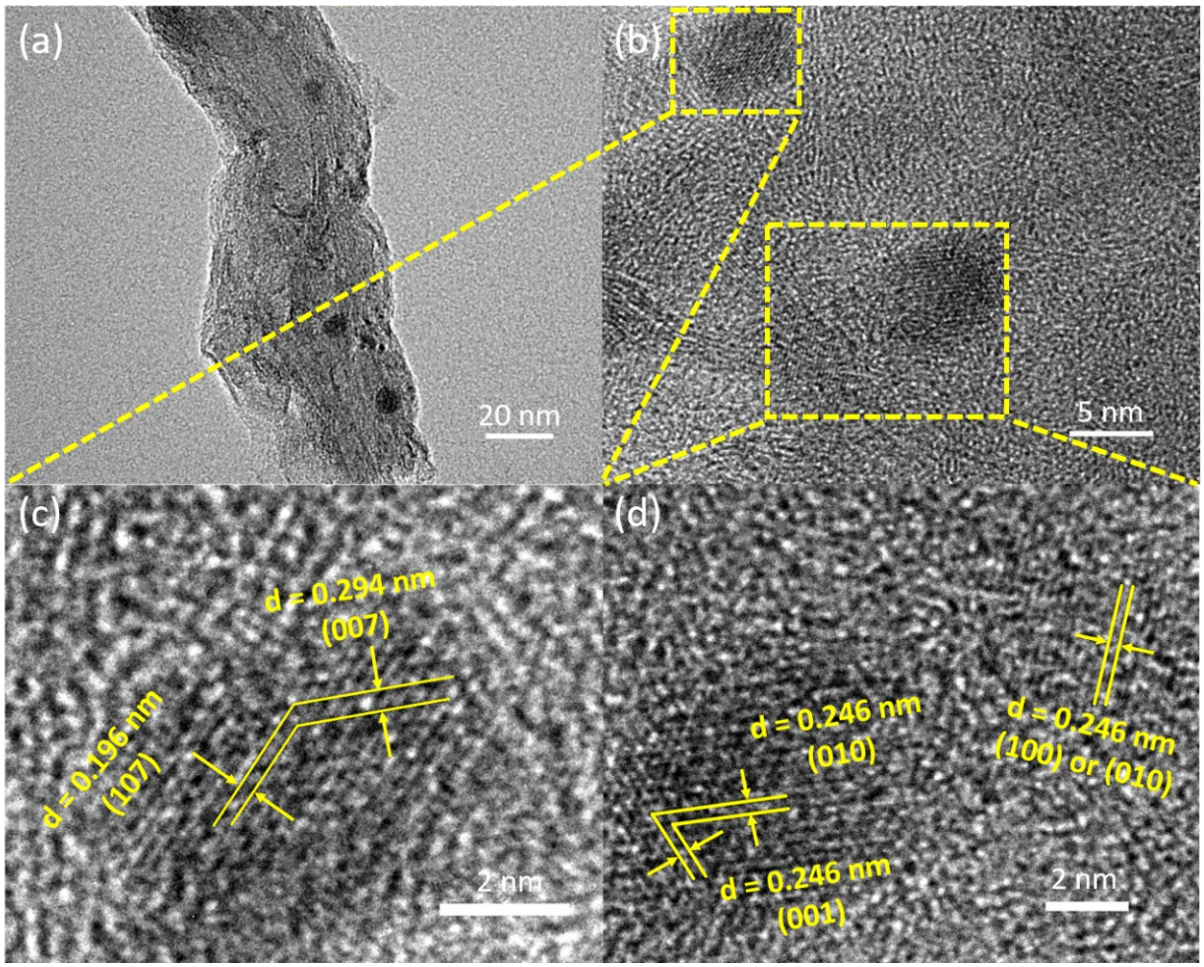

Figure S15. (a) TEM image, (b-d) HRTEM image of $Ni_{0.75}Fe_{0.25}$-P/PO_3@fCNTs after chronopotentiometry test.

The d-spacing of 0.294, 0.196 and 0.246 nm were corresponded to (007), (107) and (100) or (010) plane in *γ*-NiOOH, respectively, and it could be also speculated that *in-situ* generated Ni-Fe oxyhydroxides has not grown in preferential orientation.

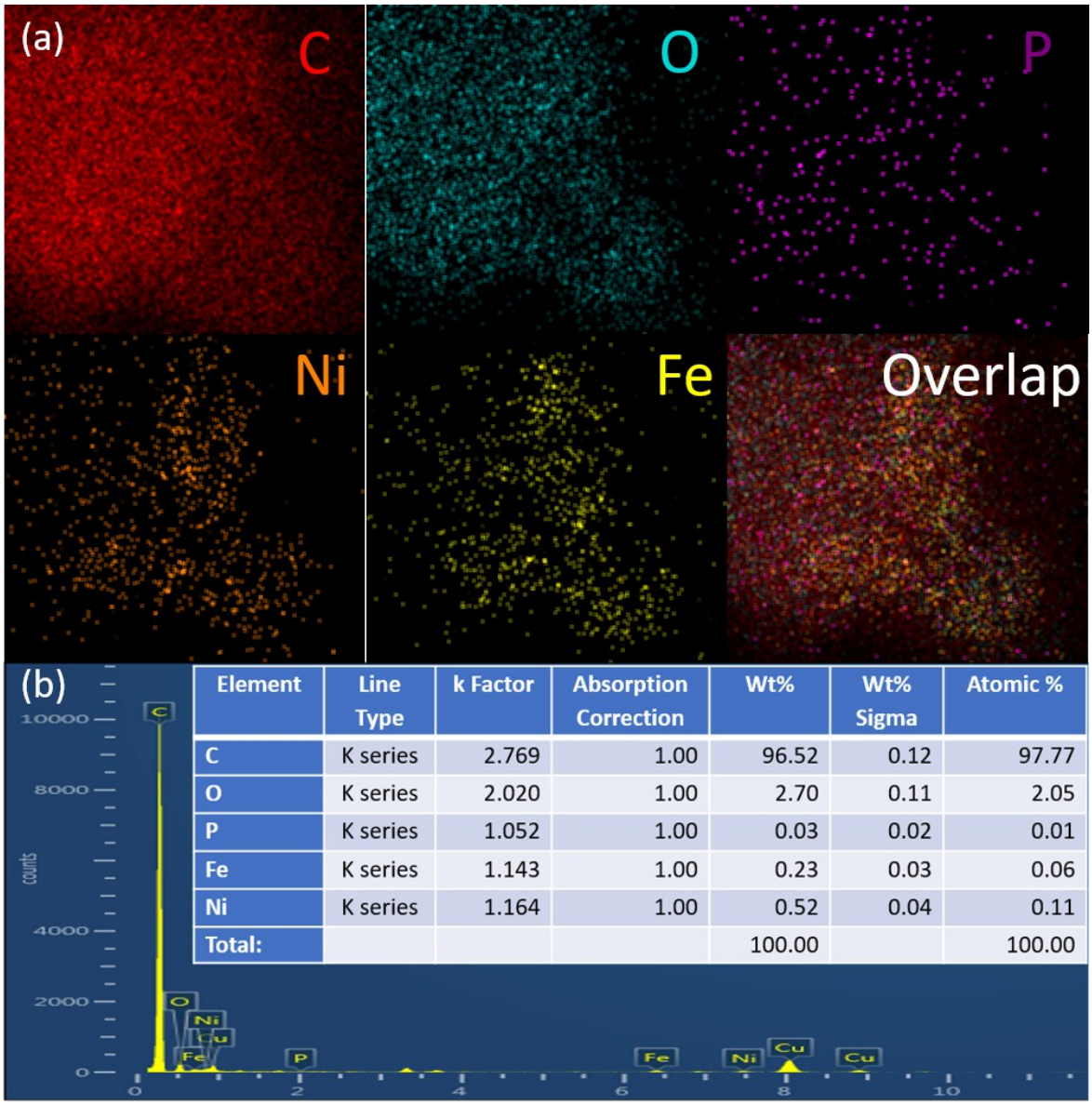

Element	Line Type	k Factor	Absorption Correction	Wt%	Wt% Sigma	Atomic %
C	K series	2.769	1.00	96.52	0.12	97.77
O	K series	2.020	1.00	2.70	0.11	2.05
P	K series	1.052	1.00	0.03	0.02	0.01
Fe	K series	1.143	1.00	0.23	0.03	0.06
Ni	K series	1.164	1.00	0.52	0.04	0.11
Total:				100.00		100.00

Figure S16. (a) EDS mapping and (b) corresponding spectrum of $Ni_{0.75}Fe_{0.25}$-P/PO_3@fCNTs after chronopotentiometry test.

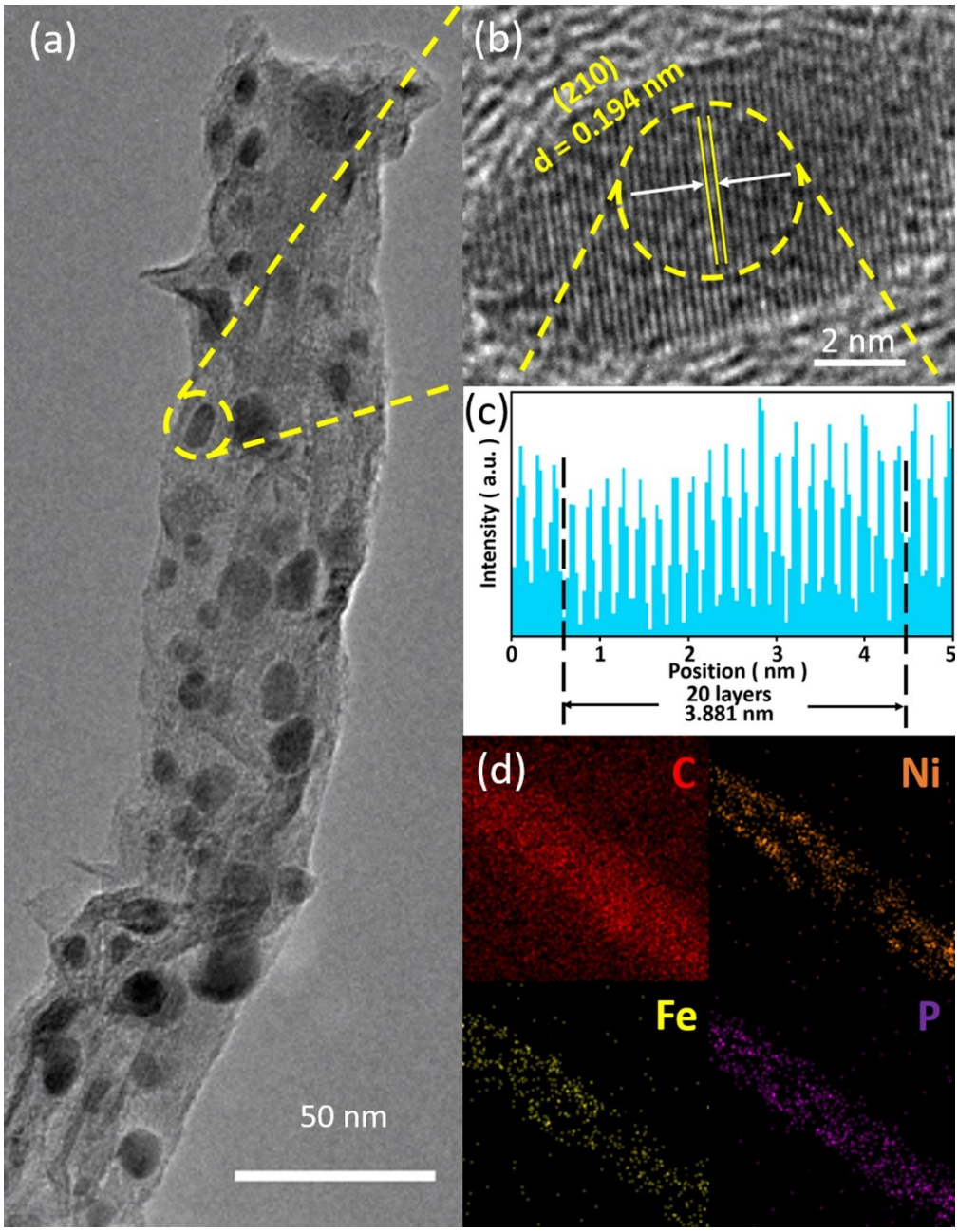

Figure S17. (a) TEM image, (b) HRTEM image and (c) corresponding lattice spacing, (d) EDS mapping of pristine $Ni_{0.75}Fe_{0.25}$-P/PO_3@fCNTs.

The high-resolution TEM image of $Ni_{0.75}Fe_{0.25}$-P/PO_3@fCNTs (**Figure S17b**) have shown clear lattice fringe with d-spacing around 0.194 nm corresponding to (210) plane of Ni_2P, which was slightly widened than the standard spacing of Ni_2P after substituting Ni atoms by Fe atoms (**Figure S17c**).

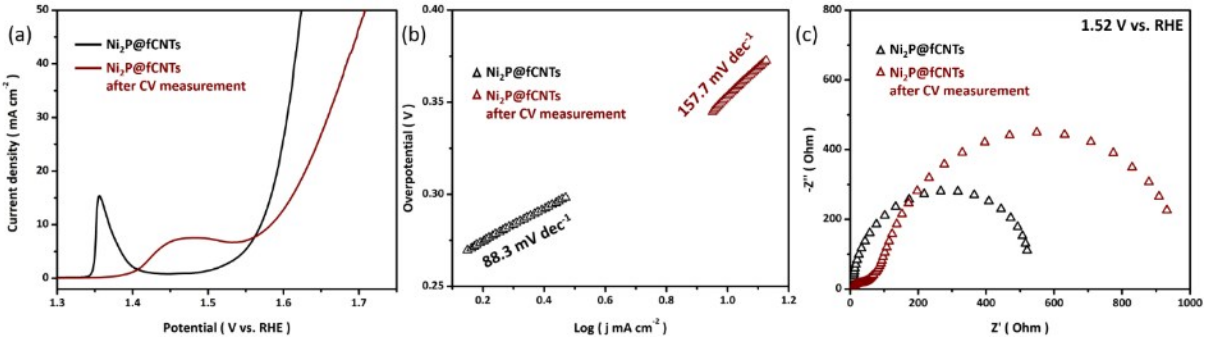

Figure S18. (a) LSV curves, (b) corresponding Tafel plots and (c) Nyquist plots of Ni_2P@fCNTs before and after CV test.

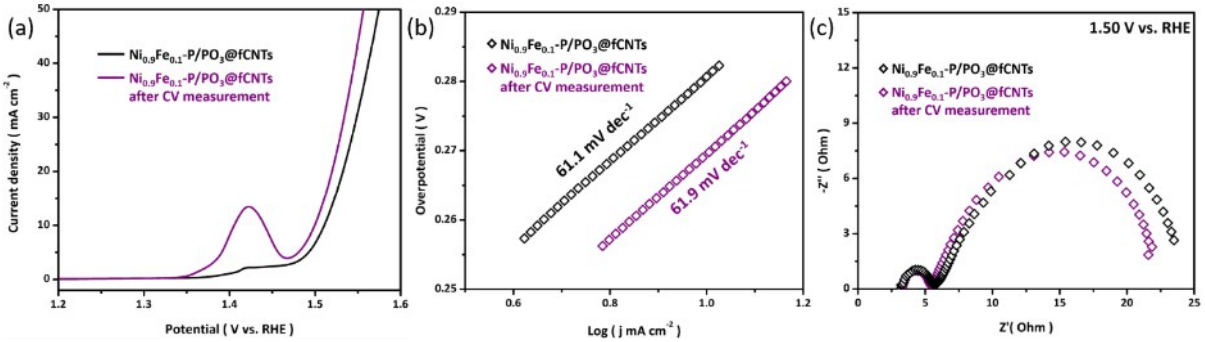

Figure S19. (a) LSV curves, (b) corresponding Tafel plots and (c) Nyquist plots of $Ni_{0.9}Fe_{0.1}$-P/PO_3@fCNTs before and after CV test.

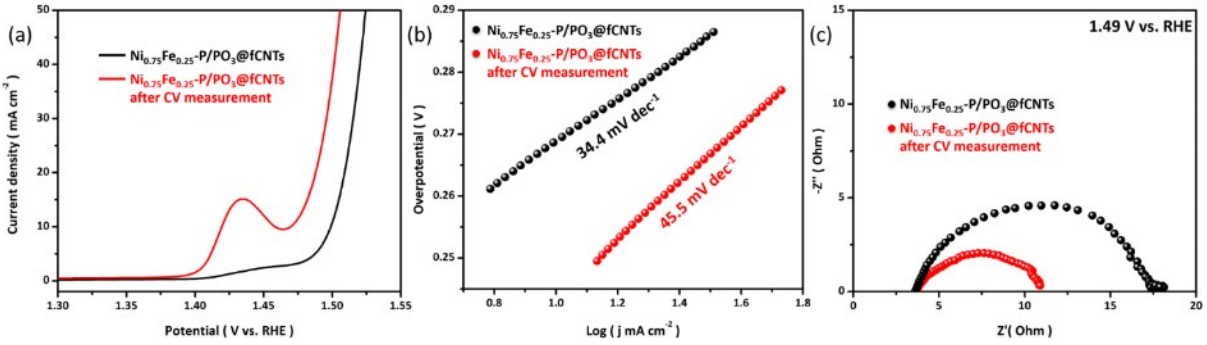

Figure S20. (a) LSV curves, (b) corresponding Tafel plots and (c) Nyquist plots of $Ni_{0.75}Fe_{0.25}$-P/PO_3@fCNTs before and after CV test.

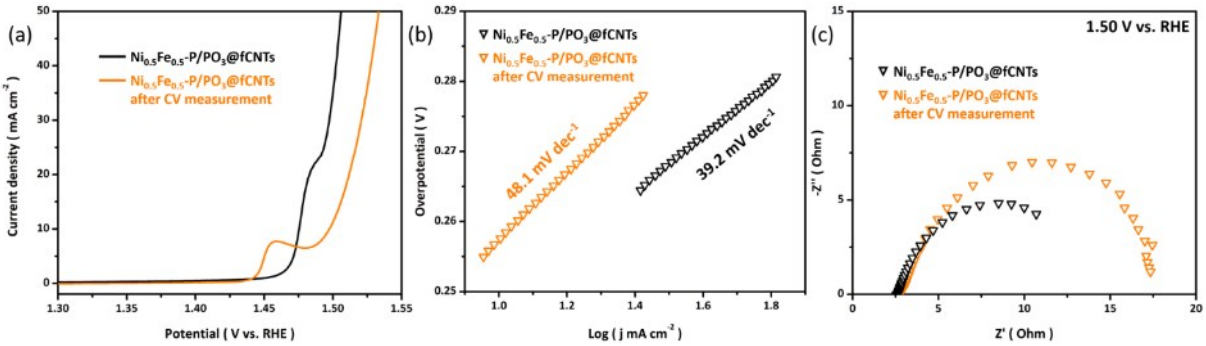

Figure S21. (a) LSV curves, (b) corresponding Tafel plots and (c) Nyquist plots of $Ni_{0.5}Fe_{0.5}$-P/PO_3@fCNTs before and after CV test.

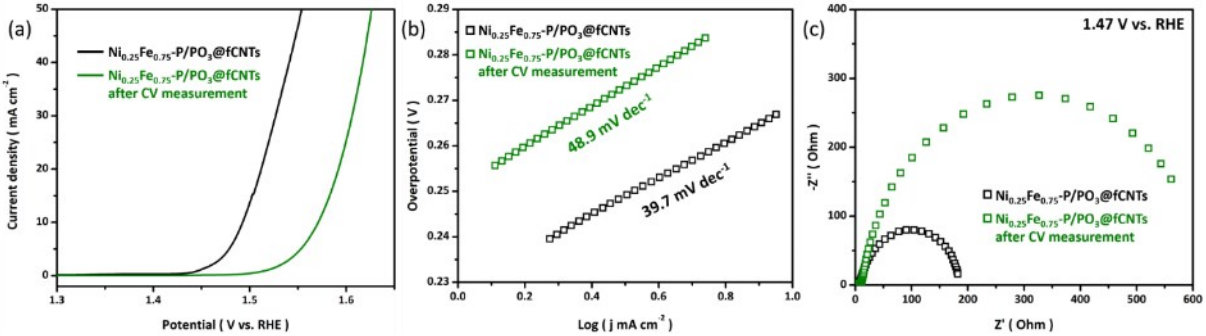

Figure S22. (a) LSV curves, (b) corresponding Tafel plots and (c) Nyquist plots of $Ni_{0.25}Fe_{0.75}$-P/PO_3@fCNTs before and after CV test.

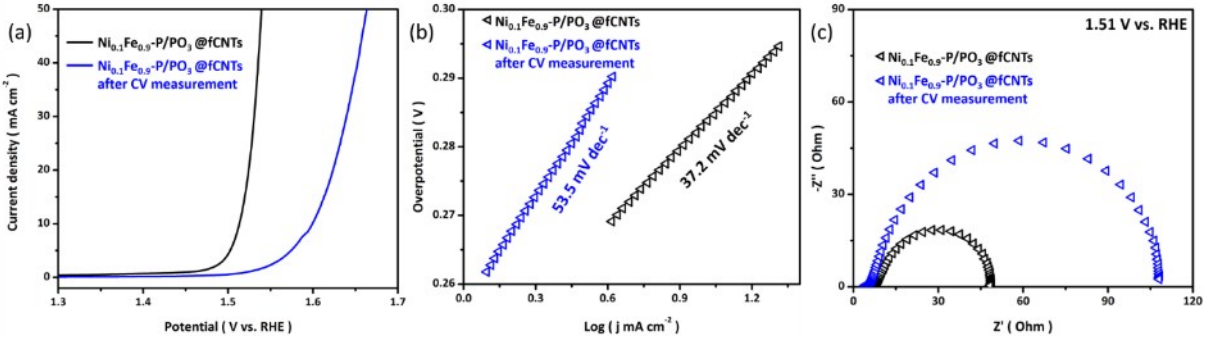

Figure S23. (a) LSV curves, (b) corresponding Tafel plots and (c) Nyquist plots of $Ni_{0.1}Fe_{0.9}$-P/PO_3@fCNTs before and after CV test.

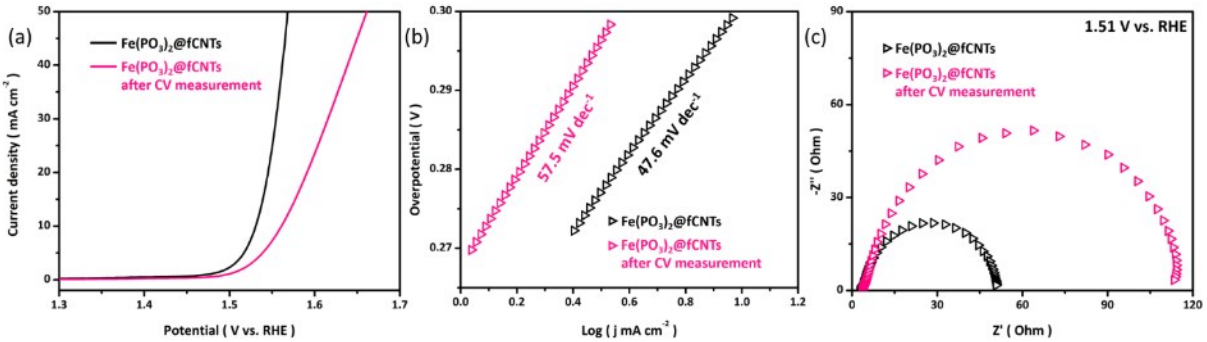

Figure S24. (a) LSV curves, (b) corresponding Tafel plots and (c) Nyquist plots of $Fe(PO_3)_2$@fCNTs before and after CV test.

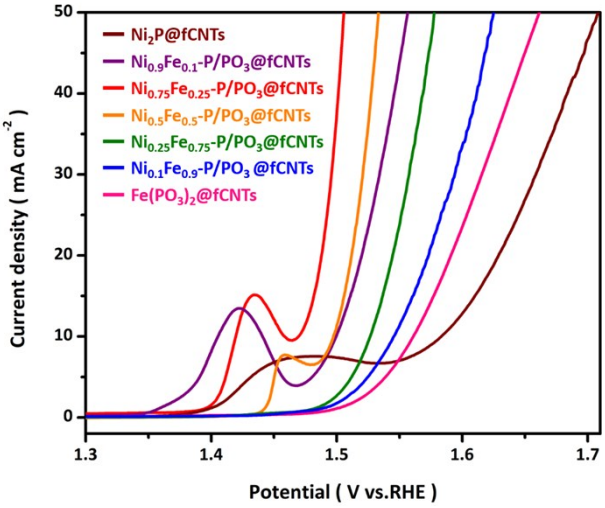

Figure S25. Comparison of LSV curves for various ratio of $Ni_{1-x}Fe_x$-P/PO_3@fCNTs catalysts after CV test.

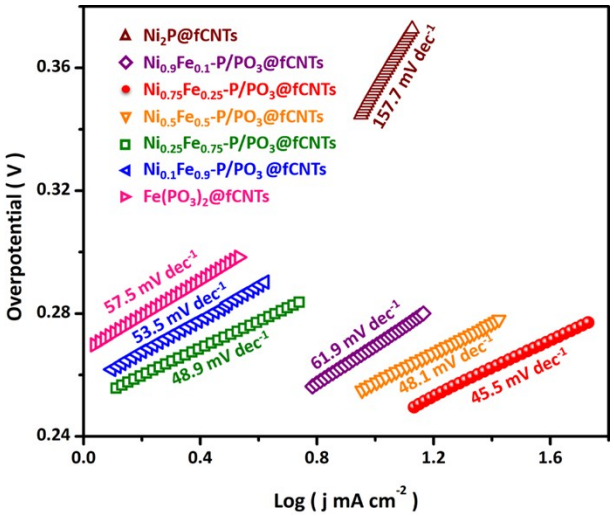

Figure S26. Comparison of Tafel plots for various ratio of $Ni_{1-x}Fe_x$-P/PO_3@fCNTs catalysts after CV test calculated from corresponding LSV curves.

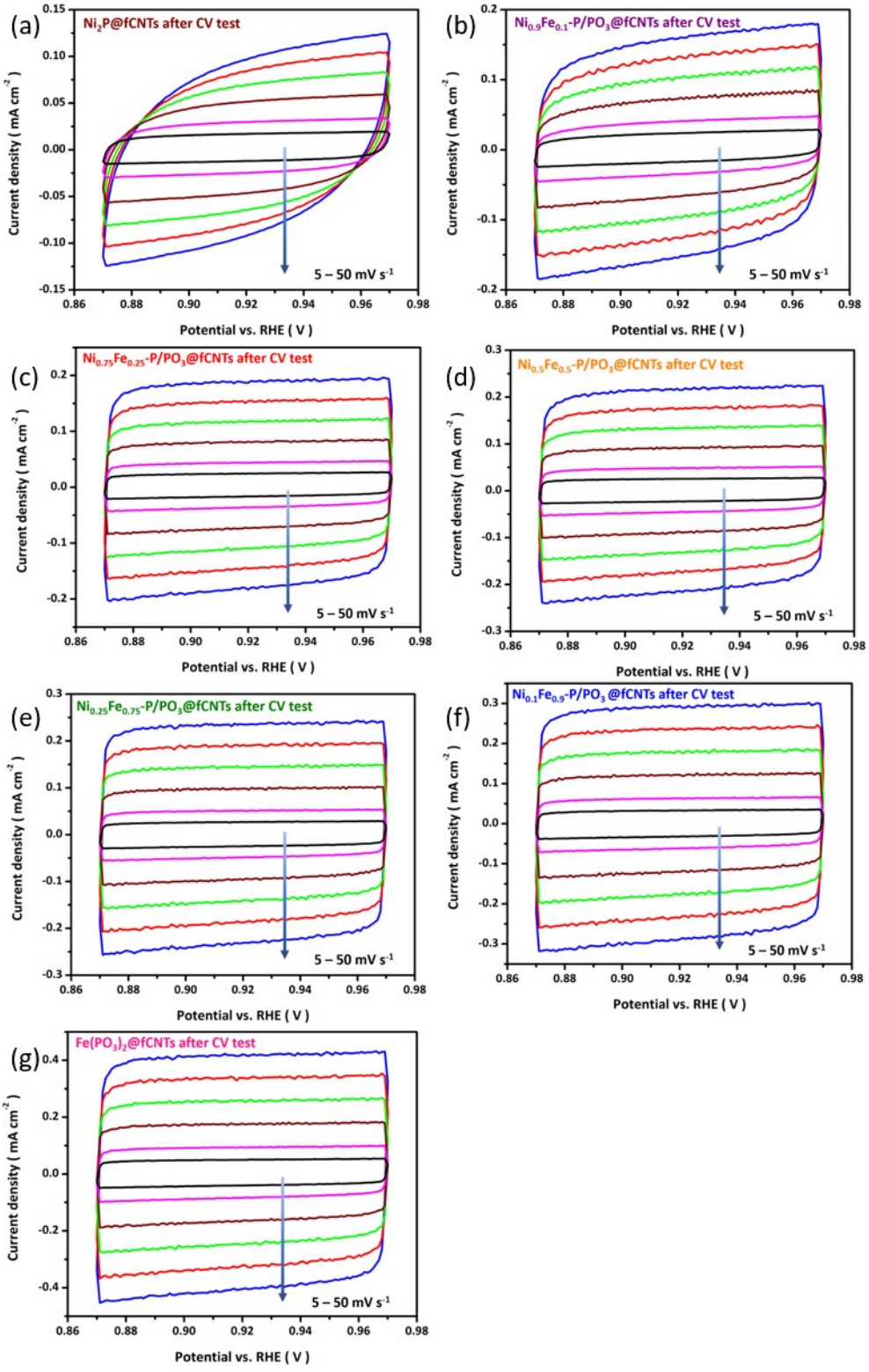

Figure S27. CV curves for various ratio of $Ni_{1-x}Fe_x$-P/PO_3@fCNTs catalysts at different scan rate from 5-50 mV s^{-1}.

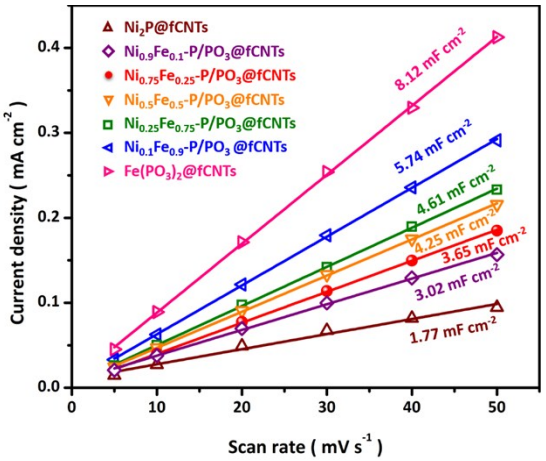

Figure S28. The difference in current density plotted against scan rate of various ratio of $Ni_{1-x}Fe_x$-P/PO_3@fCNTs catalysts to estimate the double layer capacitances.

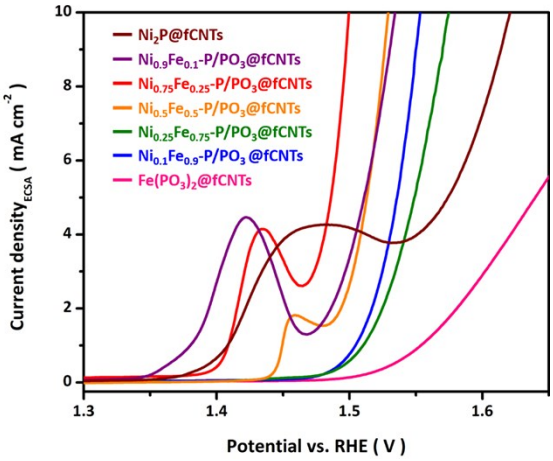

Figure S29. Polarization curves of various ratio of $Ni_{1-x}Fe_x$-P/PO_3@fCNTs catalysts normalized by ECSA.

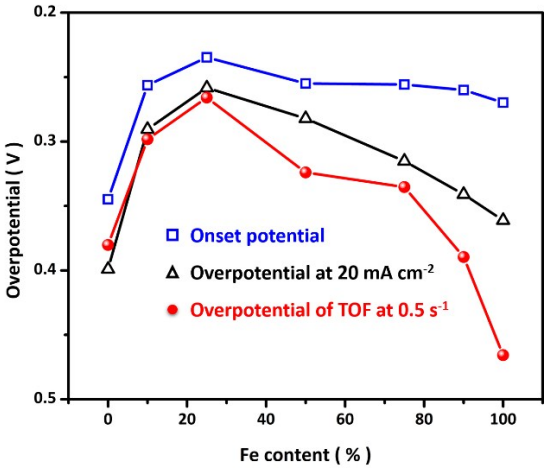

Figure S30. Comparison of onset potential, overpotential at 20 mA cm^{-2} and overpotential for TOF at 0.5 s^{-1} in various ratio of $Ni_{1-x}Fe_x$-P/PO_3@fCNTs catalysts

Table S1. Peak location of CV curves for 1st and 50th cycle with various Fe content.

Fe content (x)	oxidation peak for 1st cycle	oxidation peak for 50th cycle	reduction peak for 1st cycle	reduction peak for 50th cycle
0	1.371	1.431	1.282	1.295
0.1	1.404	1.419	1.318	1.312
0.25	1.439	1.432	1.356	1.351
0.5	1.474	1.473	1.388	1.377
0.75	1.469	1.467	1.364	1.350
0.9	1.404	1.395	1.342	1.333
1	1.390	1.409	1.326	1.322

[a)] all unit of peak location is V vs. RHE

Table S2. The relative atom ratio for O/P calculated from XPS data of $Ni_{0.75}Fe_{0.25}$-P/PO_3@fCNTs before and after electrochemical test.

$Ni_{0.75}Fe_{0.25}$-P/PO_3@fCNTs	O/P ratio (Atom %)
Pristine	0.598
after CV test	2.610
after CP test	25.187

Table S3. The concentration of electrolyte for $Ni_{0.75}Fe_{0.25}$-P/PO_3@fCNTs before and after electrochemical test measured by ICP-OES.

Sample	Fe ion concentration (mol L^{-1})	RSD* (Fe)	Ni ion concentration (mol L^{-1})	RSD* (Ni)	P ion concentration (mol L^{-1})	RSD* (P)
1 M KOH electrolyte	0	12.48	0	22.78	0	7.81
$Ni_{0.75}Fe_{0.25}$-P/PO_3@fCNTs after CV test	0	12.68	0	17.93	0.25×10^{-4}	0.62
$Ni_{0.75}Fe_{0.25}$-P/PO_3@fCNTs after CP test	3.25×10^{-7}	4.61	2.21×10^{-7}	12.65	2.70×10^{-4}	3.80
$Ni_{0.75}Fe_{0.25}$-P/PO_3@fCNTs after 200 h stability test	5.81×10^{-7}	5.70	5.11×10^{-7}	16.37	3.43×10^{-4}	3.17

*RSD: relative standard deviation

Reference cited in Supporting Information:

1. W. S. Hummers, R. E. Offeman, *J. Am. Chem. Soc.*, 1958, **80**, 1339-1339.
2. Suho Jung, Charles C. L. McCrory, Ivonne M. Ferrer, Jonas C. Peters, Thomas F. Jaramillo, J. Mater. Chem. A, 2016, **4**, 3068-3076.
3. H. Liang, A. N. Gandi, D. H. Anjum, X. Wang, U. Schwingenschlogl and H. N. Alshareef, *Nano Lett.*, 2016, **16**, 7718-7725.